Corner Vortex Structures: Large Eddy Simulations of a Confined, Premixed Bluff Body Stabilized Flame

Joshua P. Sykes[1] and Timothy P. Gallagher[2]
Innovative Scientific Solutions, Inc. Dayton, OH, 45459, USA

Christopher A. Fugger[3]
Spectral Energies, LLC, Dayton, OH, 45433, USA

Andrew W. Caswell[4] and Brent A. Rankin[5]
Air Force Research Laboratory, Wright-Patterson Air Force Base, OH, 45433, USA

The three-dimensional structure and dynamics of the recirculation zone downstream of confined, bluff-body-stabilized, turbulent, premixed flames are examined numerically. Non-reacting and reacting large eddy simulations are performed on a truncated, periodic domain and a full-span domain with spanwise walls using two mesh resolutions. The influence of spanwise walls on the size, shape, and intensity of the vortical structures in the recirculation zone are examined. The non-reacting results show that while the spanwise mean flow field is nominally uniform, turbulent statistics are sensitive to the choice of truncated or full-span domains with spanwise walls. The reacting results on the full-span domains show transverse-oriented vortices located in the corners between the bluff body trailing edge and spanwise walls. The corner vortex structures are larger than the boundary layers on the spanwise wall and can transport products into the main recirculation zone of the flow. The reacting flows show spanwise non-uniformity over the central portion of the domain typically considered to be spanwise uniform. It is recommended that future computational studies of confined bluff body stabilized flames with similar aspect ratios resolve the spanwise walls to properly model transport in the recirculation zone.

I. Introduction

Flames stabilized downstream of bluff bodies have been studied extensively because of their importance to a range of applications such as gas turbine engines. Although the geometric simplicity of confined bluff body flows makes them appealing for computational study, premixed flame stabilization downstream of a bluff body presents complex physical and chemical phenomena which can challenge the models in reacting large eddy simulations (LES). For example, different LES codes which use the same models have shown a wide range of predictions for the size and strength of the recirculation zone immediately downstream of a bluff body stabilizing a flame [1, 2].

A schematic of a representative confined bluff body flow is introduced in Fig. 1 to define a coordinate system used in the subsequent discussion. In this figure, the bluff body is a solid equilateral triangle and the aspect ratio, AR, of the bluff body is 4. The aspect ratio is defined as the spanwise extent of the flow, L, divided by the bluff body edge length, H.

[1] Research Engineer, AIAA Member.
[2] Research Engineer, AIAA Member.
[3] Research Engineer, AIAA Senior Member.
[4] Senior Research Engineer, Combustion Branch, AIAA Senior Member.
[5] Research Engineer, Combustion Branch, AIAA Senior Member.

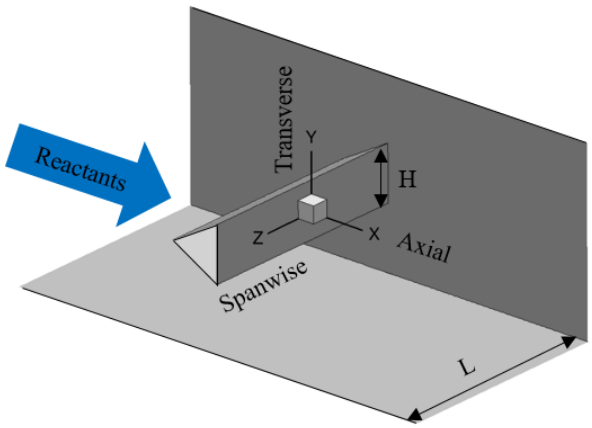

Fig. 1 Schematic of a representative bluff body with coordinate system definitions. The upper and left-hand walls are not shown.

Despite the prevalence of confined bluff body stabilized flame experiments and computations, relatively limited attention has been given to flow in the spanwise (X-Z) plane. Measurements and computations of non-reacting flows around circular bluff bodies for a range of ARs (4 - 24) have indicated the presence of strong transverse vortices in the corners of the wake near the spanwise walls [3]. The size of these corner vortex structures (CVS) is independent of AR and on the order of the bluff body cross-section characteristic length. Therefore, the CVS move away from the centerline as the bluff body aspect ratio is increased, and the mean flow field near the centerline is approximately two-dimensional [4]. Corner vortex structures are not observed in non-reacting flows around triangular bluff bodies, but the introduction of a splitter plate of sufficient length on the spanwise (X-Z) plane allows formation of CVS [5]. Bluff body flames relevant to propulsion applications operate over a similar range of Reynolds and Mach numbers as these past experiments, though the presence of reactions introduces additional flow features and interactions with possible CVS. With the exception of Schlieren imaging showing uniformity of the flame in the spanwise (X-Z) plane [6], the vast majority of measurements and computations of the bluff body reacting flows have focused on the transverse (X-Y) plane.

An example of data acquired on the transverse (X-Y) plane of a reacting bluff body flow is the work of Sjunnesson et al. [7, 8, 9], frequently referred to as the Volvo case. In this experiment, a premixed flame was stabilized downstream of a bluff body of equilateral triangular cross section (H = 0.04 m, AR = 6). Velocity [7], temperature, emissions species, lean blow out [8], and self-excited thermoacoustic mode [9] information was acquired from the X-Y plane. In recent years, a similar bluff body stabilized turbulent premixed flame has been studied at the Air Force Research Laboratory. Compared to the Volvo case, this experiment has a smaller edge length and bluff body aspect ratio (H = 0.0381 m, AR = 4). Additional details on the experiment arrangement are provided by Paxton et al. [10]. The experimental arrangement allows for laser diagnostic measurements—e.g., particle image velocimetry (PIV) and planar laser-induced fluorescence (PLIF) [11]—to be acquired in both the transverse (X-Y) and spanwise (X-Z) planes. Both of these cases have been used as validation datasets for a variety of computational studies, including the Model Validation for Propulsion (MVP) Workshop [12].

The desire to reduce computational cost often leads to simulations of a sector of the relevant physical domain, typically with periodic boundary conditions at the locations where the physical domain is truncated. While this approach requires fewer cells, it assumes that no physical flow features are larger than computational domain and may preclude resolution of important flow features. Zettervall et al. [13] simulated 1H, 2H, and 4H periodic depths of the Volvo case and suggested that resolving more than 2H in the span of the Volvo case does not substantially change flow statistics along the centerline. Giacomazzi et al. [14] visualized helicity behind the bluff body for the Volvo configuration with spanwise no-slip walls and concluded that the reacting wake is three-dimensional on an instantaneous basis; the structure noted was a series of cells stacked in the spanwise direction and having alternating helicity. Extracted velocity profiles in this study showed a variety of differences between the periodic and wall-resolved flows, leading the authors to conclude that the spanwise walls should be resolved to properly model the flow.

It is common to simulate only the central 2H spanwise region of the non-reacting and reacting bluff body flows with periodic spanwise boundary conditions. Studies which took this approach include investigations of combustion closure [15], thermoacoustic instabilities [16], and grid independence [17], among many others. A few studies [18, 19] have simulated the full span of a bluff body with a focus on the production of spanwise acoustic modes. The three-dimensional structure of the bluff body wake under stable combustion was not a primary focus of these studies.

The current work investigates the effects of spanwise walls on a confined flame stabilized on a triangular bluff body. A bluff body flame is simulated at a given operating condition with variations in:

1. Presence of spanwise walls or periodic boundary conditions
2. Presence of reactions
3. Grid refinement

Analysis of vortical features near the spanwise walls characterize their effect on the structure and dynamics of the flame and flow field—in particular, along the domain centerline.

II. Methodology

This study is conducted using a compressible, reacting LES solver (CHRIS) with a compressible flamelet formulation to model combustion [20]. Each of the flames utilize premixed propane-air, and flamelets are generated with the UC San Diego mechanism in FlameMaster [21]. Vreman's model [22] is used for subgrid-scale turbulence closure, and the flame is non-dynamically thickened such that it is resolved over at least five computational cells. The flamelet efficiency function of Charlette et al. is used to model unresolved turbulent scales in the flame [23].

Two computational domains are adapted from the experimental geometries reported by Paxton et al. [10]. Important dimensions of the computational test section are labeled in Fig. 2. The "4H" case models the entire 0.1524 m of the span and uses no-slip wall boundary conditions at the spanwise walls. The "2H" case models only the central 0.0762 m of the span and uses periodic boundary conditions at the spanwise extent. The domain extends upstream to the location of the choked backpressure plate in the experiment. Following the suggestion of the Model Validation for Propulsion workshop [12], the meshes include a plenum downstream of the test section that extends ~2 m in the axial dimension (X) and ~0.5 m in both directions of the transverse dimension (Y) to minimize the effects of the exit boundary condition on the results. In the 4H case, the plenum also extends ~0.5 m in both directions of the spanwise dimension (Z).

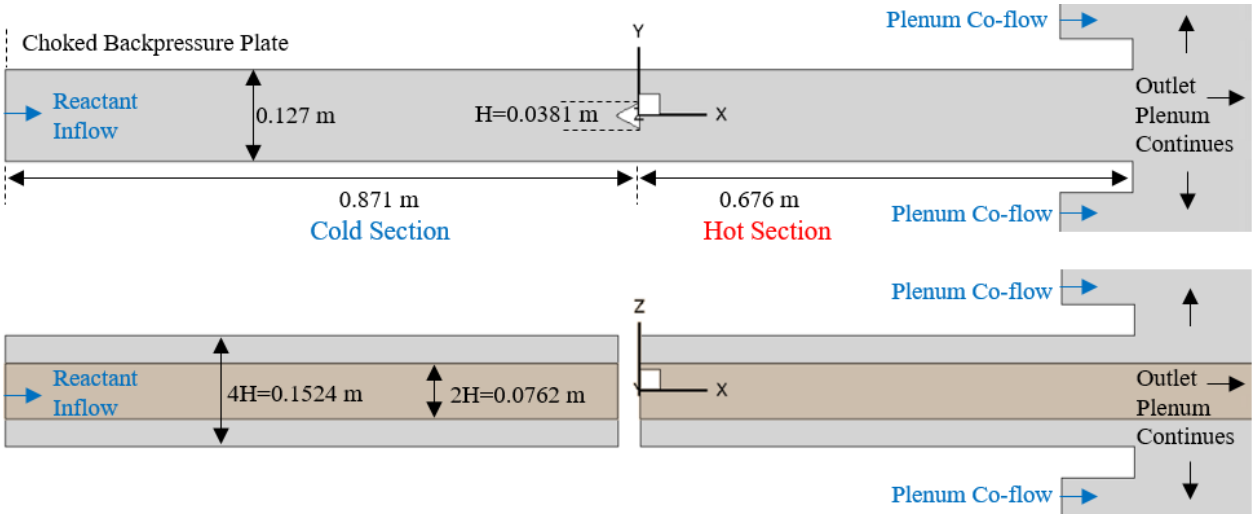

Fig. 2 Schematics of the computational domains on the transverse (top) and spanwise (bottom) planes. The 2H periodic domain is overlaid in red. Portions of the plenum are omitted from the figure.

The simulations utilize operating conditions selected to match experiments, discussed in detail by Paxton et al. [10]. The inlet is approximated as a uniform, 0% turbulent intensity non-reflective characteristic velocity inlet. In both simulation domains, the velocity is set as 16.561 m/s to match the inlet air mass flow of 0.349 kg/s for the full experimental domain. The inlet gas is a fully premixed propane/air mixture at an equivalence ratio and temperature of 0.65 and 310 K, respectively. The 1 bar static pressure outlet at the plenum exit planes uses a viscous sponge and grid stretching to reduce acoustic reflections into the domain of interest. The plenum inlet plane and sides use a low-velocity air co-flow to prevent backflow. All other boundary conditions are no-slip adiabatic walls.

Two mesh resolutions are utilized to demonstrate the sensitivity of the results to spatial resolution. The meshes are clustered near the top, bottom, and spanwise walls of the test section and along the triangular bluff body walls. Away from the walls and downstream of the bluff body, the meshes are cubic. The baseline mesh consists of nominally 4 mm cubic cells in the uniform region. Repeatedly refining by a factor of two in each dimension from this nominally

4 mm “coarse” mesh yields a nominally 2 mm “medium” mesh, a nominally 1 mm “fine” mesh, and a nominally 0.5 mm “finest” mesh. The three coarsest meshes are similar to those used by Gallagher and Sankaran [17] and the MVP guidelines [12] for the Volvo case. The fine and finest cases are not considered in this study but are generated to represent the edge of computational tractability.

A summary of the meshes considered and their resolutions of both the walls and the free stream is given in Table 1. Values of y+ are estimated from flat plate correlations. Cross-sections of the coarse 4H deep domain mesh are shown in Fig. 3. The spanwise (X-Z) plane shows that the mesh is uniform in the span direction (Z) over the central 2H section of the domain. The central 2H section is extracted and used as the mesh for the 2H cases.

Table 1 Summary of computational grids.

Name	Nominal Edge Length [mm]	Actual Freestream Edge Length [mm]	No. of Cells in 4H Domain (Millions)	No. of Cells in 2H Domain (Millions)	Bluff Body Wall y+ [nondim]	Spanwise and Transverse Wall y+ [nondim]
Coarse	4.0	3.175	3.6	1.1	20.0	24.0
Medium	2.0	1.586	28.5	8.7	10.0	12.0

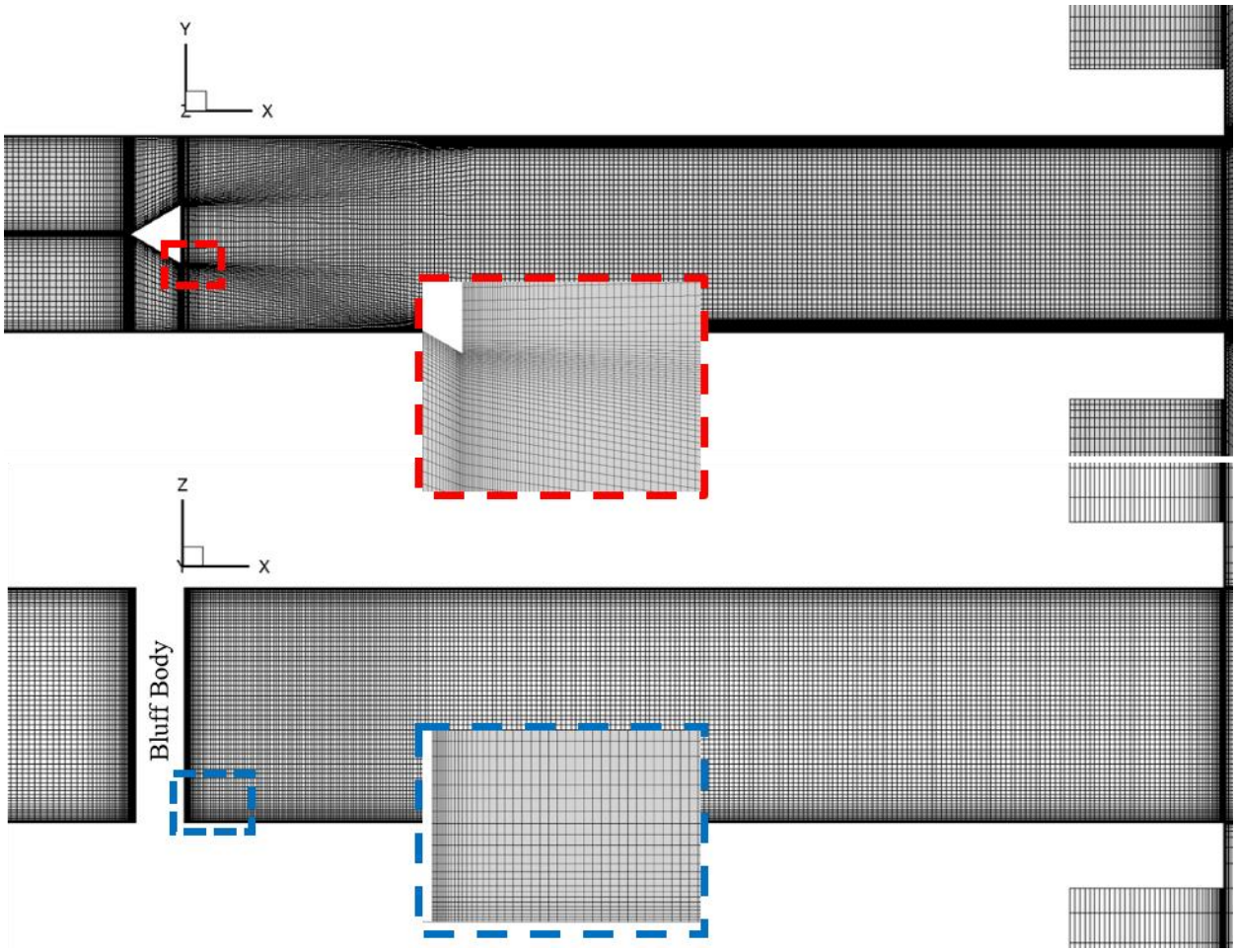

Fig. 3 Transverse (top) and spanwise (bottom) planes of the coarse mesh. Portions upstream of the bluff body and the plenum are omitted from the figure. The inserts show closer views of wall resolutions.

A summary of the cases studied in this work is given in Table 2. Each combination of three important parameters —spanwise boundary condition, grid resolution, and presence of reactions—is considered, giving a total of 8 cases. The depth and the spanwise boundary conditions are always matched, and in this work the spanwise boundary condition will be used to refer to the cases.

Table 2 Summary of operating condition, grid resolution, domain size, and spanwise boundary condition (BC) for the cases simulated in this study.

Case	Reacting	Grid	Depth	Spanwise BC
A	No	Coarse	2H	Periodic
B	No	Coarse	4H	No-slip Wall
C	No	Medium	2H	Periodic
D	No	Medium	4H	No-slip Wall
E	Yes	Coarse	2H	Periodic
F	Yes	Coarse	4H	No-slip Wall
G	Yes	Medium	2H	Periodic
H	Yes	Medium	4H	No-slip Wall

III. Results and Discussion

The non-reacting and reacting bluff body flows are analyzed through distributions of key variables, line profiles, and qualitative inspection of three-dimensional vortical structures. Mean velocity profiles are compared to preliminary PIV measurements. The PIV measurements are visually denoted by symbols, and the actual spatial resolution of the measurements is higher than that of the plotted symbols. Distances are normalized by H and the "centerline" is Y/H=Z/H=0. A detailed description of the laser diagnostics arrangement is provided by Fugger et al. [24]. Turbulence is analyzed through the anisotropy and normalized fluctuation on the centerplane using the X- and Y-velocity components as in [1]. Equation (1) defines the turbulent anisotropy as a function of the X-velocity RMS, u_{RMS}, and the Y-velocity RMS, v_{RMS}. The turbulent fluctuation level is defined by Eq. (2) in terms of the RMS velocities and the bulk velocity, U_{bulk}. Time-averaged flow velocities are typically normalized by U_{bulk}, which in these cases is 16.561 m/s. The turbulence statistics are computed over at least three flow-through times, but the velocities in the recirculation zones are slower than the bulk flow velocity and may require more time to converge statistically.

$$\text{Turbulent Anisotropy} = \frac{v_{\mathrm{RMS}}}{u_{\mathrm{RMS}}} \tag{1}$$

$$\text{Turbulent Fluctuation} = \frac{\sqrt{u_{\mathrm{RMS}}+v_{\mathrm{RMS}}}}{U_{\mathrm{bulk}}} \tag{2}$$

A. Non-Reacting Flow

Distributions of the time-averaged axial velocity for the non-reacting cases (A-D) are shown in Fig. 4. The flow is visualized over -4 < X/H < 10. In the transverse (X-Y) plane, the flow fields are qualitatively similar and show comparable sizes and intensities of the recirculation zone downstream of the bluff body. In the spanwise (X-Z) plane, the flows are uniform in the spanwise direction (apart from the thin region containing the boundary layers on the spanwise walls). The mean non-reacting flow field is qualitatively insensitive to the spanwise boundary condition (Case C vs. D) and the grid resolution (Case B vs. D).

The time-averaged vorticity provides further insight. Distributions of the vorticity, $\omega_{\mathrm{Z\,AVG}}$, orthogonal to the transverse (X-Y) plane and the vorticity, $\omega_{\mathrm{Y\,AVG}}$, orthogonal to the spanwise (Y-Z) plane are shown in Fig. 5. As with the axial velocities, the distributions of vorticity in the transverse plane are qualitatively similar. The spanwise plane shows the vorticity generated by the spanwise walls (in Cases B and D). The sign of this wall-generated vorticity switches in the region immediately downstream of the bluff body where the mean flow is reversed. This region of reversed vorticity on the spanwise walls is confined to the boundary layer, and the spanwise center of the flow shows neither coherent features nor large values of vorticity. Therefore, the periodic cases (A and C) appear representative of the spanwise centers of their corresponding no-slip wall cases (B and D, respectively).

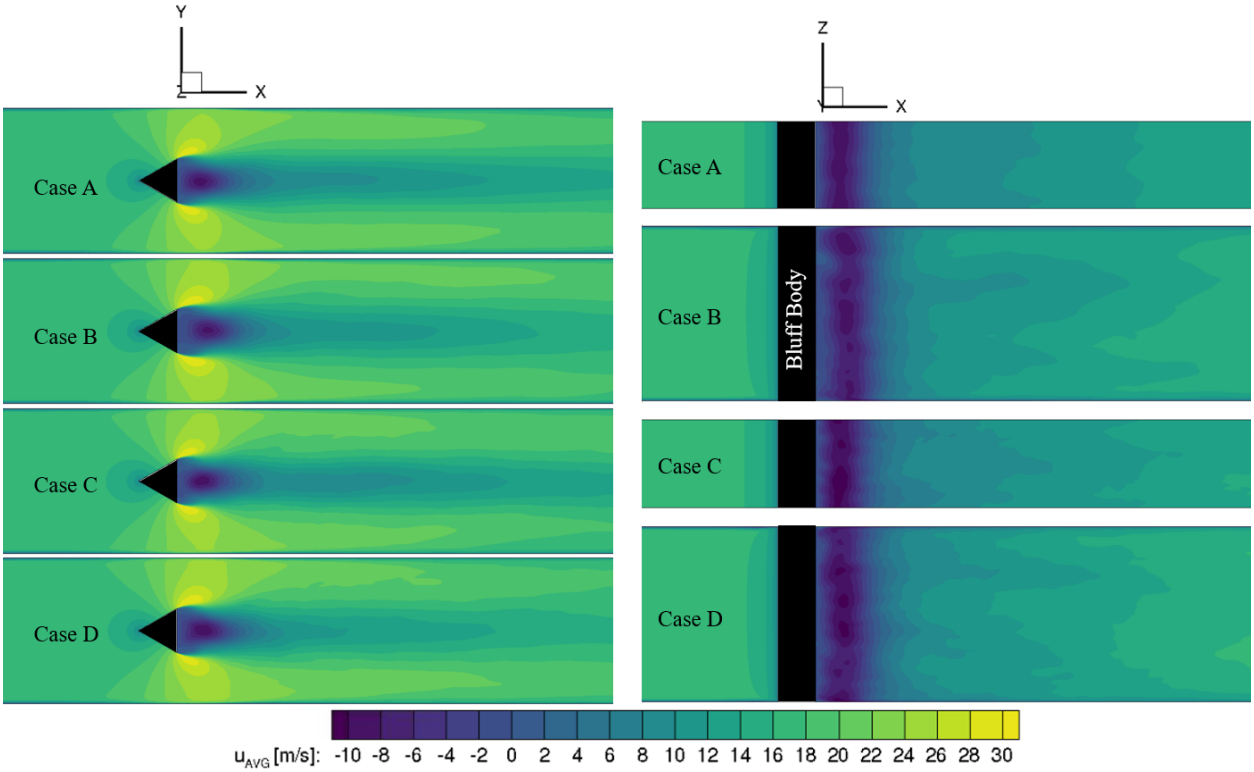

Fig. 4 Distributions of time-averaged axial velocity on the transverse (X-Y) and spanwise (X-Z) planes for simulations of non-reacting flow.

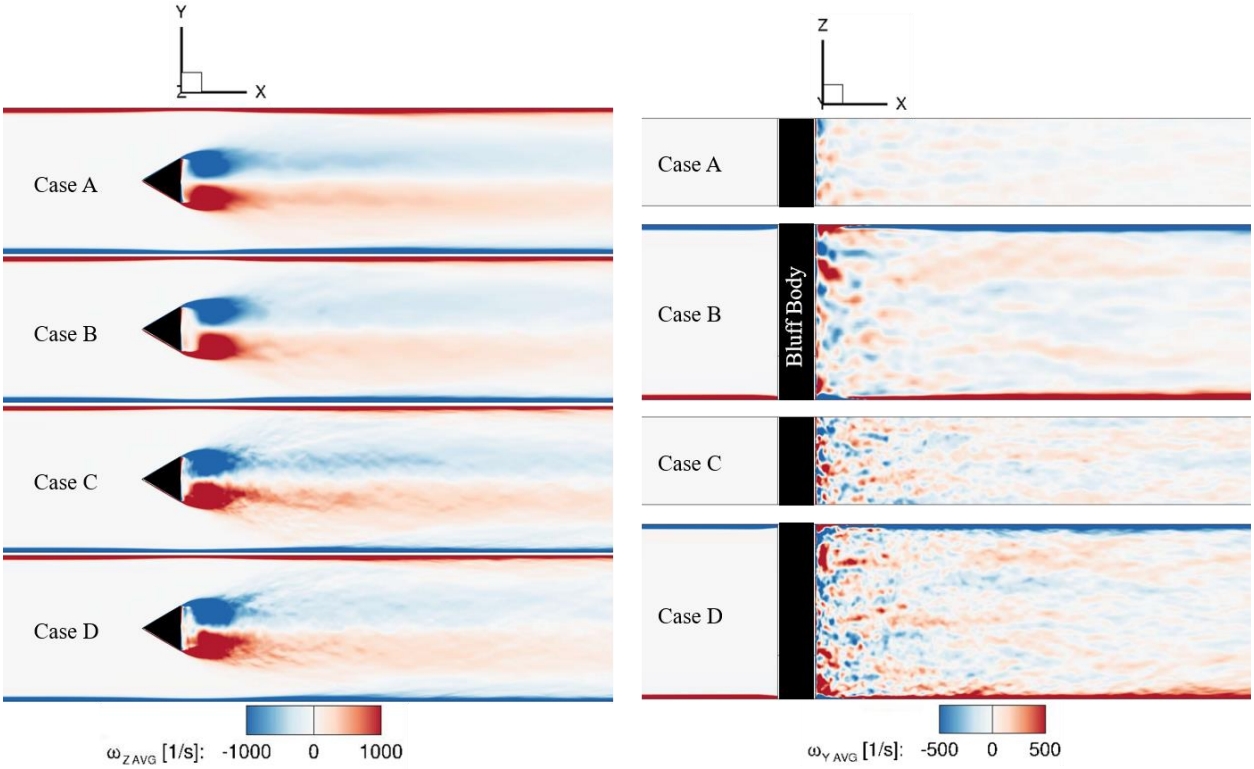

Fig. 5 Distributions of time-averaged spanwise vorticity on the transverse (X-Y) plane and transverse vorticity on the spanwise (X-Z plane) for simulations of non-reacting flow.

The effect of any spanwise non-uniformity on the non-reacting flow is further considered through mean flow and turbulent statistics at the centerline, historically the most common evaluation metrics in bluff body flows. Fig. 6 plots the non-dimensional axial velocity, turbulent anisotropy, and turbulent fluctuation along the centerline for the non-reacting cases (A-D). The non-dimensional axial velocity profiles show that, within the recirculation zone, fewer differences are caused by the boundary conditions on the medium mesh (Case C vs. D) than on the coarse mesh (Case A vs. B). As the recirculation zone closes, the influence of the boundary condition becomes more important as the two wall cases (B and D) cluster together as do the two periodic cases (A and C). The cases with walls (B and D) show better agreement with the PIV measurements downstream of the recirculation zone. Although the simulations fail to capture the correct recirculation zone strength (error ~25%), defined as the minimum value of the mean axial velocity, the results of all considered cases show good agreement with the PIV in the recirculation zone length.

Within the recirculation zone, the cases with walls (B and D) show lower anisotropy values than the periodic cases (A and C), showing sensitivity of the turbulence to the spanwise boundary conditions even at the centerline. Downstream of the recirculation zone, there are no clear trends in the anisotropy values with regard to the grid resolutions and domain sizes considered. The cases with walls (B and D) generally show lower turbulent fluctuations in the recirculation zone than the periodic cases (A and C), but the variation is insignificant downstream. The non-reacting turbulent quantities show sensitivity to the spanwise boundary conditions and the choice of those conditions should be considered in future validation efforts.

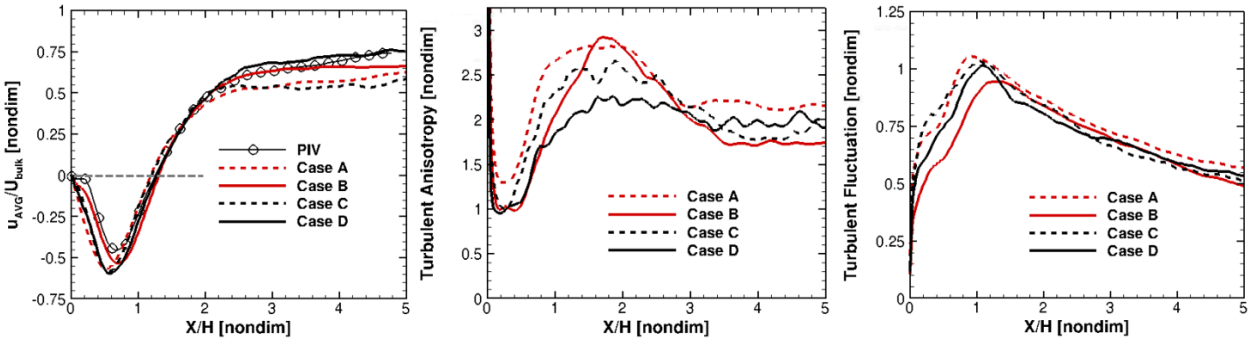

Fig. 6 Simulated and measured centerline profiles of time-averaged axial velocity (left), turbulent anisotropy (center), and turbulent fluctuation (right) for non-reacting flow. The close of the recirculation zone is where the velocity profiles cross the gray reference line.

B. Reacting Flow

Distributions of the instantaneous temperature, *T*, for the reacting cases (E-H) are shown in Fig. 7. The flame in the coarse mesh cases (E and F) shows little evidence of Kelvin-Helmholtz roll-up at the bluff body trailing edge, whereas wrinkling in this area is evident in the medium mesh cases (G and H). On the 4mm coarse mesh, the thickened flame model thickens the resolved flame front approximately 100 times thicker than the laminar flame thickness, meaning that the range of modeled turbulent scales in the flow is large. Qualitatively, the effect of the choice of boundary condition in the coarse grid cases (E vs. F) does not have a dramatic effect on the flame topology and the flame brush is located in roughly the same position. In the medium mesh case, however, the choice of spanwise walls noticeably affects the qualitative topology of the flame and the convection of necked features is more prevalent in the periodic case (G) than in the case with walls (H). Reacting flow simulations which use periodic boundary conditions show qualitatively different flow features from a simulation with the spanwise walls resolved.

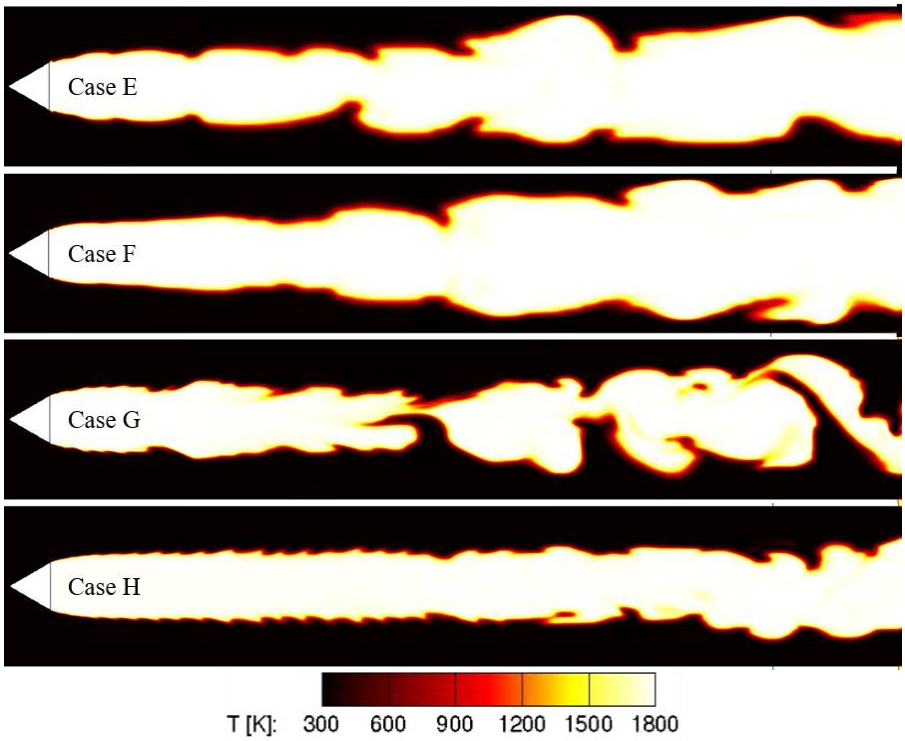

Fig. 7 Distributions of instantaneous temperature on the transverse (X-Y) plane for simulations of reacting flow.

Distributions of time-averaged axial velocity for the reacting cases (E-H) are illustrated in Fig. 8. With the introduction of reactions, the flow field is highly sensitive to both the choice of grid refinement (Case E vs. Case G and Case F vs. Case H) and the spanwise boundary condition (Case E vs. Case F and Case G vs. Case H). The recirculation zones of the medium cases (G and H) are longer than those of the coarse cases (E and F). In the region immediately downstream of the bluff body, the medium mesh velocities are so low that the region can be described as either a recirculation zone or a wake—that is, a region without coherent spanwise vortical structure. Both of types of structures have been observed in previous simulations of bluff body flows [1, 25], but experimental observations are of the recirculation type. For both resolutions, the cases with walls (F and H) show significant spanwise non-uniformity of the flow. Immediately downstream of the bluff body, the axial velocity is positive near the spanwise walls and negative in the spanwise center of the flow. This non-uniformity persists downstream and the contours of velocity beyond the recirculation zone curve such that they are nearer the bluff body at the spanwise walls than in the depthwise center of the flow. This spanwise non-uniformity of the velocity field cannot be captured by simulations when using periodic boundary conditions.

Distributions of vorticity for the reacting cases are plotted in Fig. 9. The shorter recirculation zones of the coarse mesh cases (E and F) means that spanwise vorticity switching due to baroclinic torque happens at approximately X/H=7 whereas this occurs downstream of the visualized region in the medium mesh cases (G and H). In the spanwise (X-Z) plane, the periodic cases (E and G) do not show any coherent transverse vortical structures. The coarse case with walls (F), however, shows a pair of large, coherent transverse vortices in the recirculation zone. The sign of the vorticity of these features is consistent with the spanwise wall boundary layers within the region of negative axial velocity (as in Cases B and D in Fig. 5). In moving from the end of the recirculation zone to the bluff body trailing edge, the regions of transverse vorticity roll up and become larger in the span (on the order of H). The magnitude of the vorticity in these CVS is lower in the case H, likely as a result of the lower-velocity recirculation zone in that case leading to smaller gradients. The magnitude and size of the CVS are qualitatively similar to those observed by PIV and chemiluminescence of the transverse (X-Z) plane in the experiment [24].

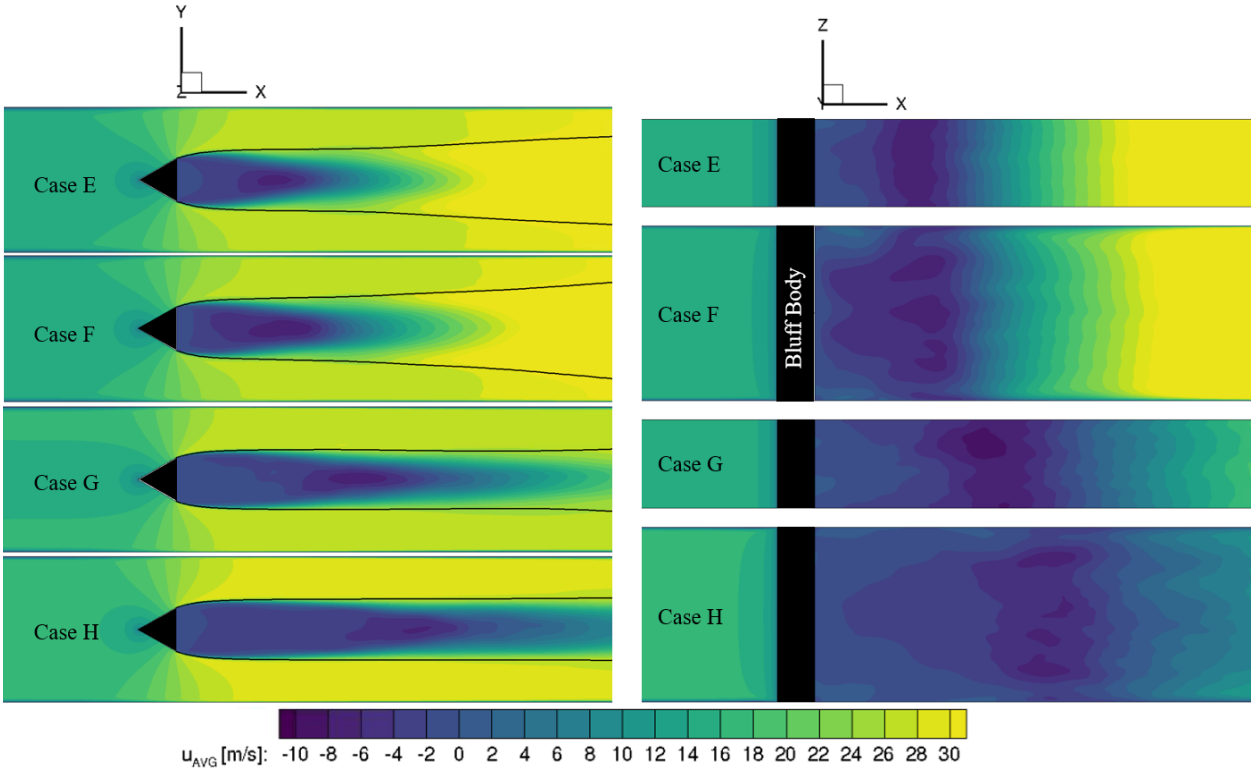

Fig. 8 Distributions of time-averaged axial velocity on the transverse (X-Y) and spanwise (X-Z) planes for simulations of reacting flow. The mean flame position based on maximum temperature gradient is overlaid as a black line in the transverse plane.

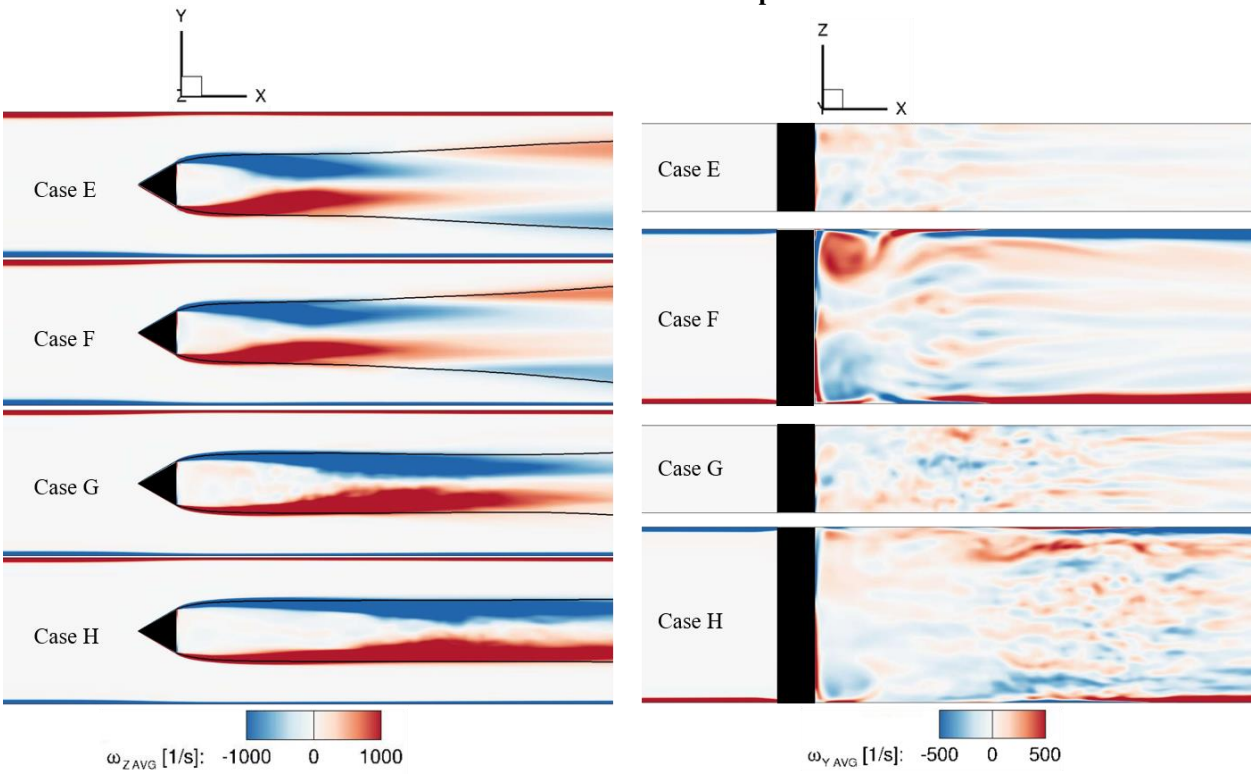

Fig. 9 Distributions of time-averaged spanwise vorticity on the transverse (X-Y) plane and transverse vorticity on the spanwise (X-Z) plane for simulations of reacting flow. The mean flame position based on maximum temperature gradient is overlaid as a black line in the transverse plane.

The effect of the CVS on the reacting flow is characterized by centerline profiles of the non-dimensional axial velocity, turbulent anisotropy, and turbulent fluctuation in Fig. 10. The coarse mesh cases (E and F) do not capture the intensity of the recirculation but approximate the length of the recirculation zone within 10%. After the end of the recirculation zone the coarse mesh cases over-predict the axial flow velocity. The medium mesh cases (G and H) over-predict the length of the recirculation zone but appear to show an accurate rate of increasing velocity thereafter. Both meshes show that spanwise wall effects extend the recirculation zone. Downstream of the recirculation zone, the centerline velocities of the cases with spanwise walls (F and H) are reduced compared to the periodic cases (E and G), but this may be due to the extended recirculation zones offsetting the start of flow acceleration. As in the non-reacting cases, the spanwise walls result in a decreased level of turbulent fluctuation, at least within the recirculation zone. The same clustering between cases with similar boundary conditions is present in the values of turbulent anisotropy—that is, cases with walls (F and H) show anisotropy values closer to 0.75 outside of the recirculation zone while the periodic cases do not show this trend. Similar to many other studies, simulation on different grids show a wide variety of recirculation zone lengths and intensities [1, 2]. The resolution of the spanwise walls in the reacting bluff body flow has a non-negligible effect on the centerline profiles of mean and turbulent quantities.

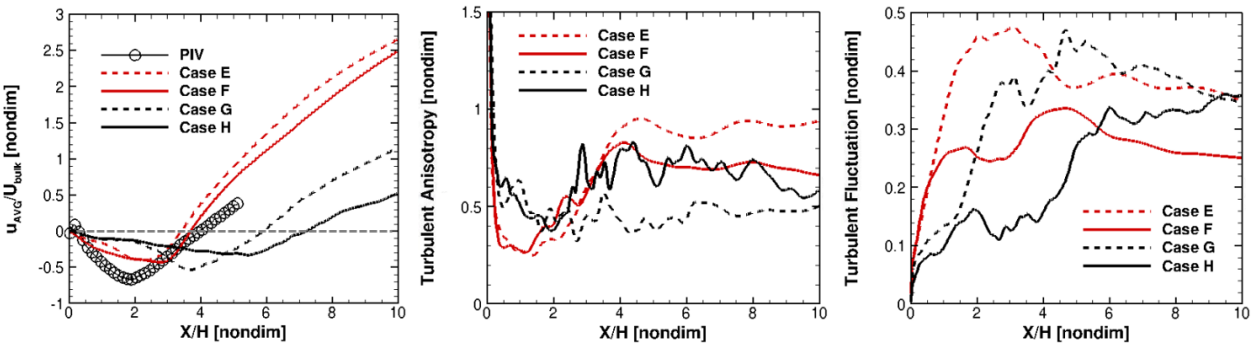

Fig. 10 Simulated and measured centerline profiles of time-averaged axial velocity (left), turbulent anisotropy (center), and turbulent fluctuation (right) for reacting flow. The close of the recirculation zone is where the velocity profiles cross the gray reference line.

C. Reacting Recirculation Zone Structure

Having seen that the CVS affect the flow along the domain centerline, the mechanism for this effect is now sought. Streamlines from the mean flow in the reacting cases with walls (F and H) are shown in Fig. 11. Seed points for the streamlines are placed in the CVS region at X/H=1, Y/H=0, and |Z/H|>1. These points are illustrated as black spheres. Any volume traced by the streamlines will have interacted with flow not modeled in the periodic 2H domain. The streamlines are colored by the ratio between the local spanwise and transverse mean vorticities, $|\omega_{Z\,AVG}|/|\omega_{Y\,AVG}|$. The streamlines interacting only with the spanwise (X-Z) plane will have a value of 0, and the streamlines interacting only with the transverse (X-Y) plane will have an infinite value. This metric primarily serves to illustrate the three-dimensionality of a given streamline as fluid moves between the transverse and spanwise planes.

By tracing backwards in time, the reactant flow into the CVS can be observed. This is most apparent in Case H, where the fluid originates in the boundary layers on the spanwise walls, crosses the flame sheet, reacts, and is entrained into the CVS. Moving forward in time, the fluid in the CVS displays the transverse vortical motion observed in Fig. 9. Eventually, the fluid turns in the axial direction and displays primarily spanwise vortical motion—that is, participation in the main recirculation zone. While this turning is happening, the fluid moves towards the spanwise centerline. Ultimately the products from the CVS mix with the other products in the spanwise center of the flow and convect downstream; this occurs in both mesh resolutions (Cases F and H) despite the weaker recirculation zone of Case H. The streamlines suggest that the CVS and the primary spanwise vortices in the recirculation zone are part of a large, connected structure which transports products from the spanwise walls to the centerline of the flow.

Additional visualization of the three-dimensionality of the flow is provided by an isosurface of the Q-criterion for each reacting case in Fig. 12. The value of the Q-criterion for the isosurface is arbitrarily chosen to allow visualization of the CVS without obstruction from other small features. The isosurfaces are colored by the ratio of vorticities described previously. The recirculation zone is visible in all cases as a green (spanwise vorticity) feature which extends from the trailing edge of the bluff body to further downstream. In the cases with walls (F and H), the CVS are visible as blue structures immediately downstream of the bluff body. The CVS extends transversely into the shear layer at the bluff body trailing edge and at their junction the vorticity transitions from transverse to spanwise. This observation

supports the hypothesis that the CVS and primary spanwise vortices connect to provide a mechanism for three-dimensional transport of products.

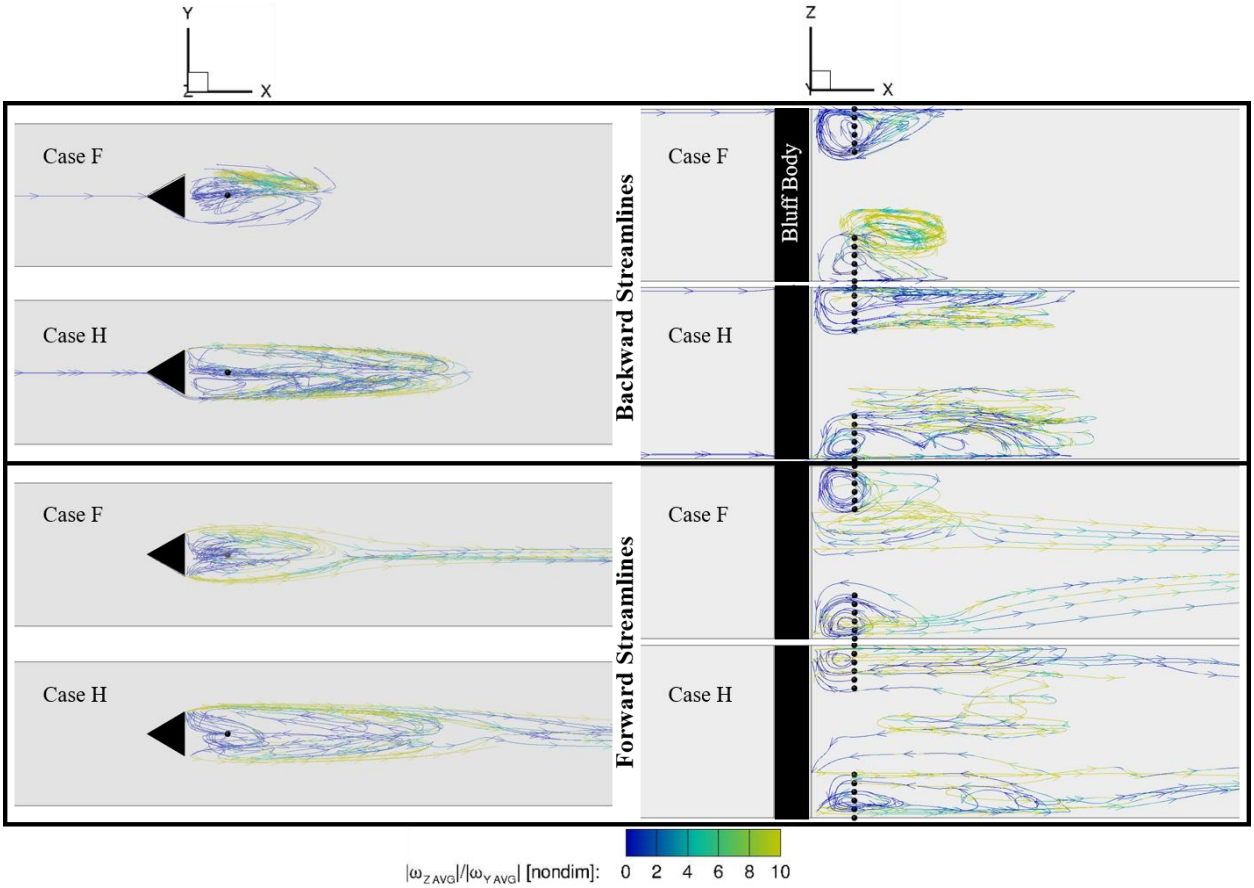

Fig. 11 Streamlines of fluid entering (top) and exiting (bottom) the corner vortex structures based on the time-average velocity distributions for the reacting flow. The streamlines are seeded at the black spheres and traced backward (top) and forward (bottom) in time. The streamlines are colored by the ratio of the transverse to spanwise vorticity.

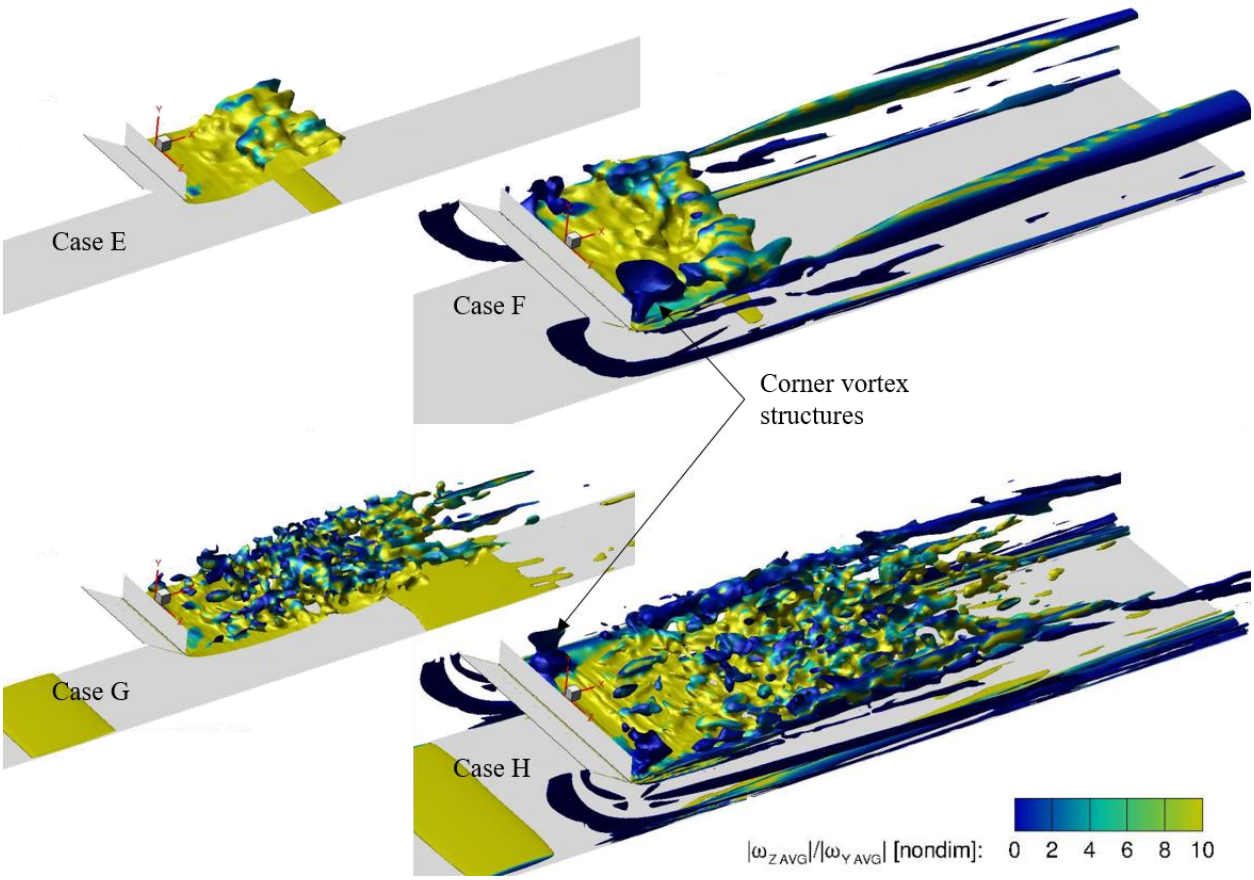

Fig. 12 Reacting case isosurfaces of Q-criterion colored by participation in either transverse or spanwise vortical structures. Only the bottom half of the domain is visualized to reveal the corner vortex structures.

IV. Concluding Remarks

Large eddy simulations are used to explore the effects of spanwise wall resolution and reactions on confined bluff body flows and verify experimental observations of spanwise non-uniformity. Results indicate that although the spanwise mean flow field of the non-reacting flow is uniform, resolution of the spanwise walls affects the centerline turbulent statistics, particularly in the recirculation zone. The reacting flows are not uniform in the spanwise direction and display coherent, transverse vortical structures adjacent to the bluff body trailing edge and spanwise walls. These corner vortex structures are sized on the order of the bluff body edge length and interact with the dominant flow direction through transport of products. Spanwise non-uniformity of the flow field is observed within the central 2H of the span, and the turbulent statistics of the reacting wake vary as a function of mesh resolution and the spanwise boundary condition.

The resolution of spanwise walls results in different vortical structures between the non-reacting and reacting flows around the triangular bluff body, but in both cases the walls affect the centerline flow. The size of the CVS and their effect of spanwise non-uniformity on the reacting bluff body flow suggest that future computational studies of confined bluff body stabilized flames should resolve the spanwise walls to properly model the recirculation zone.

Acknowledgments

This work is based on research sponsored by the Air Force Research Laboratory. The first two authors are supported by contract number FA8650-19-F-2046 and the third author is supported by contract number FA8650-15-

D-2518. Computational resources have been provided by the Department of Defense High-Performance Computing Modernization Program. This work has been approved for public release; distribution unlimited (88ABW-2019-5654).

References

[1] P. A. T. Cocks, V. Sankaran and M. C. Soteriou, "Is LES of Reacting Flows Predictive? Part 1: Impact of Numerics," in *AIAA SciTech Forum*, Grapevine, TX, 2013.
doi: 10.2514/6.2013-170

[2] A. Comer, M. Ihme, C. Li, S. Menon, J. Oefelein, B. Rankin, V. Sankaran and V. Sankaran, "Proceedings of the First Model Validation for Propulsion (MVP 1) Workshop," Model Validation for Propuls, 9-13 January 2017. [Online]. Available: https://community.apan.org/wg/afrlcg/mvpws/p/proceedings. [Accessed 25 November 2019].

[3] N. A. Ozturk, A. Akkoca and B. Sahin, "PIV Measurements of Flow Past a Confined Cylinder," *Experiments in Fluids*, vol. 44, 2008.
doi: 10.1007/s00348-007-0459-z

[4] H. Strandenes, B. Pettersen, H. I. Andersson and M. Manhart, "Influence of Spanwise No-Slip Boundary Conditions on the Flow Around a Cylinder," *Computers and Fluids*, vol. 156, 2017.
doi: 10.1016/j.compfluid.2017.06.025

[5] C. L. Ford and P. M. Winroth, "On the Scaling and Toplogy of Confined Bluff-Body Flows," *Journal of Fluid Mechanics*, vol. 876, pp. 1018-1040, 2019.
doi: 10.1017/jfm.2019.583

[6] E. E. Zukoski, "Flame Stabilization on Bluff Bodies at Low and Intermediate Reynolds Numbers," Ph.D. Dissertation, Engineering and Applied Science Dept., California Institute of Technology, Pasadena, CA, 1954.

[7] A. Sjunnesson, C. Nelsson and E. Max, "LDA Measurements of Velocities and Turbulence in a Bluff Body Stabilized Flame," *Laser Anemometry*, vol. 3, pp. 83-90, 1991.

[8] A. Sjunnesson, S. Olovsson and B. Sjoblom, "Validation Rig - A Tool for Flame Studies," in *ISABE Conference*, Nottingham, UK, 1991.

[9] A. Sjunnesson, P. Henrikson and C. Lofstrom, "CARS Measurements and Visualization of Reacting Flows in a Bluff Body Stabilized Flame," in *Joint Propulsion Conference*, Nashville, TN, 1992.
doi: 10.2514/6.1992-3650

[10] B. Paxton, C. A. Fugger, B. A. Rankin and A. W. Caswell, "Development and Characterization of an Experimental Arrangement for Studying Bluff-Body-Stabilized Turbulent Premixed Propane-Air Flames," in *AIAA SciTech Forum*, San Diego, CA, 2019.
doi: 10.2514/6.2019-0118

[11] C. A. Fugger, S. Roy, B. A. Rankin, A. W. Caswell and J. R. Gord, "Structure and Dynamics of CH2O, OH, and the Velocity Field of a Confined Bluff-Body Premixed Flame," *Proceedings of the Combustion Institute*, vol. 37, pp. 1461-1469, 2019.
doi: 10.1016/j.proci.2018.05.014

[12] A. Comer, "3rd Model Validation for Propulsion Workshop Overview and Validation Cases," 8 June 2018. [Online]. Available: https://community.apan.org/wg/afrlcg/mvpws/p/cases. [Accessed 25 November 2019].

[13] N. Zettervall, K. Nordin-Bates, E. J. K. Nilsson and K. Fureby, "Large Eddy Simulation of a Premixed Bluff Body Stabilized Flame Using Global and Skeletal Reaction Mechanisms," *Combustion and Flame*, vol. 179, pp. 1-22, 2017.
doi: 10.1016/j.combustflame.2016.12.007

[14] E. Giacomazzi, V. Battaglia and C. Bruno, "The Coupling of Turbulence and Chemistry in a Premixed Bluff-Body Flame as Studied by LES," *Combustion and Flame*, vol. 138, pp. 320-335, 2004.
doi: 10.1016/j.combustflame.2004.06.004

[15] S. Pope and J. Kim, "Effects of Combined Dimension Reduction and Tabulation on the Simulations of a Turbulent Premixed Flame Using a Large-Eddy Simulation/Probability Density Function Method," *Combusion Theory and Modeling*, vol. 18, no. 3, pp. 388-413, 2014.
doi: 10.1080/13647830.2014.919411

[16] H.-G. Li, P. Khare and H.-G. Y. V. Sung, "A Large-Eddy-Simulation Study of Combustion Dynamics of Bluff-Body Stabilized Flames," *Combustion Science and Technology*, vol. 188, no. 6, pp. 924-952, 2016.
doi: 10.1080/00102202.2015.1136296

[17] T. P. Gallagher and V. Sankaran, "Affordable Explicitly Filtered Large-Eddy Simulation for Reacting Flows," *AIAA Journal*, vol. 57, no. 2, pp. 809-823, 2019.
doi: 10.2514/1.J057213

[18] B. Rochette, F. Collin, D. Maestro, A. Ghani, O. Vermorel, L. Gicquel and T. Poinsot, "Influence of Acoustic, Chemistry Description and Wall Heat Transfer in LES of the Volvo Bluff-Body Stabilized Flame Dynamics," in *AIAA SciTech Forum*, Grapevine, TX, 2017.

[19] A. Ghani, T. Poinsot, L. Gicquel and G. Staffelbach, "LES of Longitudinal and Transverse Self-excited Combustion Instabilities in a Bluff-Body Stabilized Turbulent Premixed Flame," *Combustion and Flame*, vol. 162, no. 11, pp. 4075-4083, 2015.
doi: 10.1016/j.combustflame.2015.08.024

[20] A. Saghafian, L. Shunn, D. A. Philips and F. Ham, "Large Eddy Simulations of the HIFiRE Scramjet Using a Compressible Flamelet/Progress Variable Approach," *Proceedings of the Combustion Institute*, vol. 35, pp. 2163-2172, 2015. doi: 10.1016/j.proci.2014.10.004

[21] "Chemical-Kinetic Mechanisms for Combustion Applications," San Diego Mechanism web page, Mechanical and Aerospace Engineering (Combustion Research), University of California at San Diego, [Online]. Available: http://combustion.ucsd.edu.

[22] A. W. Vreman, "An Eddy-Viscosity Subgrid-Scale Model for Turbulent Shear Flow: Algebraic Theory and Applications," *Physics of Fluids*, vol. 16, pp. 3670-3681, 2004. doi: 10.1063/1.1785131

[23] F. Charlette, C. Meneveau and D. Veynante, "A Power-Law Wrinkling Model for LES of Premixed Turbulent Combustion Part I: Non-Dynamic Formulation and Initial Tests," *Combustion and Flame*, vol. 131, pp. 159-180, 2002. doi: 10.1016/S0010-2180(02)00400-5

[24] C. A. Fugger, J. P. Sykes, T. P. Gallagher and A. W. Caswell, "Corner Vortex Structures: Spanwise Imaging of a Confined, Premixed Bluff Body Stabilized Flame," in *AIAA SciTech Forum*, Orlando, FL, 2020 (to be published).

[25] V. Sankaran and T. P. Gallagher, "A Consistent Reactive LES Based on Explicit Filtering," in *AIAA SciTech Forum*, San Diego, CA, 2019. doi: 10.2514/6.2019-0451